Kaon production in nucleus-nucleus collisions at 92 MeV per nucleon

R. Legrain,[1] J. F. Lecolley,[2] F. R. Lecolley,[3] N. Alamanos,[1] L. Bianchi,[3] Y. Cassagnou,[1] H. Dabrowski,[4] B. Erazmus,[4] J. Julien,[1,4] D. Lebrun,[5] Ch. Le Brun,[2] A. Mougeot,[1] P. Hameau,[1] G. Perrin,[5] P. de Saintignon,[5] J. L. Sida,[1] and J. P. Wieleczko[3]

[1]*DAPNIA/SPhN, CEA/Saclay, F-91191 Gif-sur-Yvette Cedex, France*

[2]*LPC, ISMRA et Université de Caen, CNRS/IN2P3, 6 bld du Maréchal Juin, 14050 Caen Cedex, France*

[3]*GANIL, BP 5027, F-14021 Caen Cedex, France*

[4]*SUBATECH, Université de Nantes/Ecole des Mines de Nantes, CNRS/IN2P3 4 rue Alfred Kastler, La Chantrerie, 44072 Nantes Cedex 03, France*

[5]*ISN Grenoble, 53 Avenue des Martyrs, F-38026 Grenoble Cedex, France*

(Received 31 July 1998)

K^+ production far below the free nucleon-nucleon threshold has been investigated in collisions of ^{36}Ar on ^{12}C, ^{nat}Ti, and ^{181}Ta targets at an incident energy of 92 MeV per nucleon. The cross sections for K^+ production have been inferred from the observed muon decays of positive kaons. The results are discussed in the framework of a participant-spectator model and are compared to proton induced K^+ production and to subthreshold pion production experiments. [S0556-2813(99)00303-9]

PACS number(s): 25.70.−z, 25.75.Dw

I. INTRODUCTION

Meson production in heavy ion collisions at subthreshold energies offers the possibility to study dense and hot nuclear systems and thus possibly the underlying nuclear equation of state [1]. At incident energies per nucleon well below the free nucleon-nucleon threshold, nucleons have to undergo several collisions in the hot and compressed zone to gain by chance enough energy to allow meson production, or in a cooperative model, several nucleons have to pool their energy to produce the particles. Both processes are density and temperature dependent; so meson production can be a good probe of the early stages of the collision if the particle can escape the interaction zone without substantial final state interaction. In that respect kaons, and especially K^+, seem to be particularly suitable since they have extremely low absorption and a small scattering cross section with nucleons. K^+ production, in the elementary process $N+N \rightarrow K^+ + \Lambda + N$, requires an available energy of $E_0 = 670$ MeV, that is to say, 1.58 GeV, for an incident nucleon on a fixed target or 335 MeV for each nucleon. This makes K^+ production by first-chance nucleon-nucleon collisions very unlikely at incident energies around 100 MeV/nucleon for which it has been shown that the pion production is in agreement with the simple participant-spectator collision geometry [2,3].

Another interest in K^+ production comes from the intrinsic nature of the kaon, since its production requires the joint production of a pair of strange quarks. Therefore subthreshold experiments on strangeness production may be related to the low but significant strange quark component in nucleons [4–6]. It is thus interesting to compare pion and kaon production in the same energetic conditions.

The production of K^+ was measured more than ten years ago in Ne+NaF collisions at 2.1 GeV per nucleon [7], and only few data exist at subthreshold energies. An enhanced K^+ production compared to microscopic transport calculations has been found in ^{197}Au+^{197}Au collisions at 1 GeV/nucleon [8]. Our earlier measurement of K^+ production in ^{36}Ar+^{nat}Ti at 92 MeV/nucleon [9] is up to now the only result at an energy far below the free nucleon-nucleon threshold. The order of magnitude of the cross section is in reasonable agreement with the systematics of meson production probabilities per participant nucleon as a function of the Coulomb-corrected bombarding energy, normalized to the production threshold in free nucleon-nucleon collisions [10]. It has also been reproduced by two quite different theoretical calculations. One of these calculations was performed in the framework of a cooperative model which has already been applied to subthreshold pion production [11], while the other assumed an incoherent production mechanism and introduced fluctuations using the Boltzmann-Langevin approach with a soft equation of state [12].

In this paper, we report on new measurements of K^+ production using a beam of 92 MeV/nucleon ^{36}Ar. The experiment is described in Sec. II. The data analysis methods are presented in Sec. III and the results are discussed in Sec. IV.

II. EXPERIMENTAL DETAILS

A. Kaon detection

In K^+ production measurements in heavy ion collisions around 100 MeV per nucleon, the K^+ energy is low and it is not possible to use magnetic detection and range telescope techniques as at higher incident energies. However, it is still possible to detect kaon decays with no kaon energy threshold. In this case, a total production cross section can only be inferred while the angular distribution and the kaon energy cannot be measured.

The mean lifetime of the K^+ is 12.4 ns and the main decay channels are (i) $K^+ \rightarrow \mu^+ \nu$ with a branching ratio of 64% and a muon kinetic energy $T_{\mu^+} = 153$ MeV for a decay at rest and (ii) $K^+ \rightarrow \pi^+ \pi^0$ with a branching ratio of 21% and a pion kinetic energy $T_{\pi^+} = 110$ MeV for a decay at rest. The delayed particle (μ^+ or π^+) is detected in a range

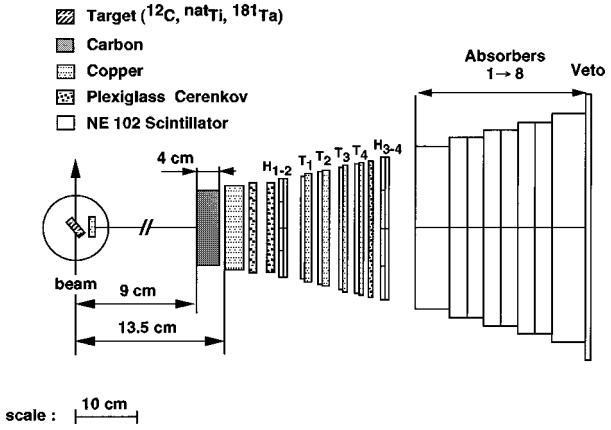

FIG. 1. Sketch of the experimental apparatus. Hodoscopes were labeled H, triggers T. Different materials are represented by different shading as indicated.

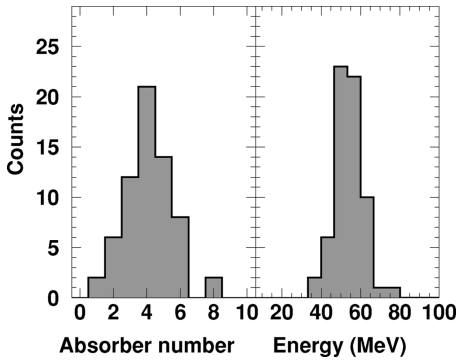

FIG. 2. Simulation of the range and energy deposited in the absorbers for muons coming from the disintegration of K^+.

telescope designed to accommodate a high counting rate. Since the branching ratio is higher for the muon decay channel and the range of a 153 MeV muon is larger than the range of a 110 MeV pion, there is an enhanced rejection of wrong events. The emission of kaons can be tagged by the range and energy measurement of the delayed 153 MeV muons. The mean lifetime measurement provides an additional check. This method takes advantage of two interesting characteristics of the GANIL beams: the very high intensity available on a small beam spot (a few mm^2) and a well-defined time structure (1 ns every 70 ns) which allows the measurement out of the beam burst with a reasonable number of triggers. The same detection method was used in the first K^+ production experiment performed at GANIL [9] while the same kaon decay method was used in proton induced K^+ production measurements [13].

B. Experimental setup

The experimental setup is shown schematically in Fig. 1. A copper plate to stop kaons up to 40 MeV energy for normal trajectories was located 1.5 cm from the center of the target, covering polar angles from 45° to 135°. Muons from the kaon decays were detected in a range telescope located at 90 ° with respect to the beam direction.

The telescope was made of passive and active absorbers and consisted of four parts.

(1) Passive absorbers of different nature, placed in front of the telescope in order to reduce the background counting rate in the first active planes.

(2) The trigger (T1–4) where a coincidence between the detection planes was required, and the trajectories could be checked in two hodoscopes (H1,2, H3,4). Plates of copper were inserted between the trigger detectors in order to enlarge the matter thickness. The first trigger plane (T1,23 cm$\times$23 cm) was located 25.5 cm from the target. The four active trigger planes were segmented in forward and backward parts.

(3) Just behind, the muons of interest were stopped in the eight absorbers (A1–A8, 2 and 4 cm thick), allowing the measurement of the range, the specific energy loss and the residual energy of stopping particles. The absorber planes were segmented in four parts.

(4) The last detection plane provided a veto to reject energetic cosmic muons crossing the whole telescope.

All detectors were tuned and energy calibrated using cosmic-ray muons.

C. Simulation

The whole detector geometry was put into a simulation using the GEANT package from the CERN library [14]. The emission of the kaons was assumed to be isotropic from the center of the target. Muons from the decay of kaons were then selected and tracked trough the detector. The energy loss spectra of all scintillators were constructed. The resulting range and energy distributions are shown on Fig. 2 for the expected experimental statistics. The total energy detected in the active parts of the telescope ($\simeq$55 MeV) is a significant part of the muon energy (153 MeV). The total efficiency of the detection system has been extracted from this simulation for different velocities and energy distributions of the primary kaon source. The simulation yielded a total efficiency around 0.7%. More details on the results of these calculations will be given in Sec. IV.

D. Experiment

The experiment has been performed at the GANIL National Laboratory using a $\simeq$200 nA ^{36}Ar beam and ^{12}C, ^{nat}Ti, and ^{181}Ta targets 102 mg/cm^2, 92 mg/cm^2, and 79 mg/cm^2 thick, respectively. The range telescope was centered at 90 ° with respect to the beam direction. The beam pipe and some mechanical parts close to the target were made of low-Z material in order to limit the background counting rate. A parasitic beam was used to determine the nature, thickness, and position of the absorbers in front of the telescope and in between the trigger planes. Several configurations have been tested. The final configuration was chosen in order to accommodate the highest beam current with the lowest counting rate. The on-line trigger condition required the coincidence between the H3-4, T1, T2, T3, T4, and A1 planes. A time measurement of the trigger plane T3 with respect to the beam time structure (accelerator RF) was performed. The timing of the Cyclotron RF was checked continuously with an independent scintillator. For each target,

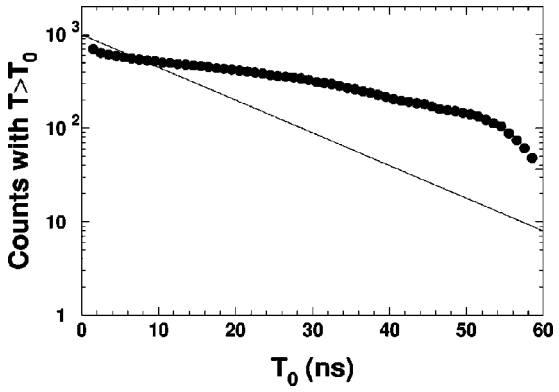

FIG. 3. Time distribution obtained after the first selection (see text). The solid line corresponds to the time decay of K^+. This selection is insufficient to extract the muons correlated to this decay.

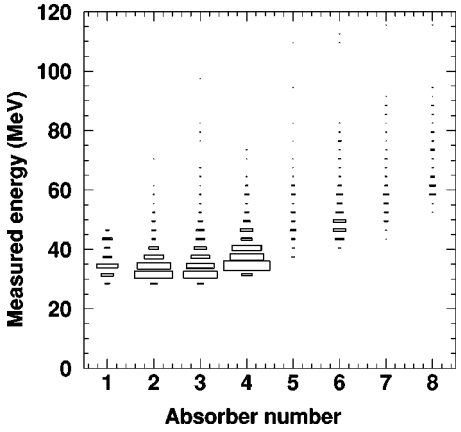

FIG. 4. Measured energy loss versus absorber depth for the events selected in the first stage of the analysis. The size of each box is proportional to the number of counts in the corresponding bin.

data were accumulated with a gate that rejected prompt events, but runs including prompt events were performed periodically.

III. DATA ANALYSIS

A. Events selection

The muonic kaon decay events were identified by using the energy loss information from the telescope. At each step of the analysis, the time distribution of the selected events was compared to the kaon decay. The off-line data reduction was performed in two steps, with most of the background events being rejected in the first stage by the following selections.

(1) Only delayed particles, with time arrival into the T3 counters larger than at least 3 ns with respect to the beam spill were considered, to reject prompt events.

(2) A narrow time coincidence was applied to all planes, to reject random events.

(3) The measured energy losses in each counter of the trigger part were required to be inside an energy window defined on the lower part by the cosmic muon at the minimum of ionization and on the higher part by the values calculated for protons.

(4) The triggering conditions were still satisfied when requiring only one hit per detection plane.

This first selection yielded about 700 events for the three targets. The time distribution of these events is shown in Fig. 3 as the remnant population of events after a delayed time T_0. The solid line represents the expected slope for kaon decay. It is clear that the selection of kaon decay events from the background has to be more efficient.

Figure 4 shows the measured energy loss versus the absorber depth for the events selected in the first stage of the analysis. The energy threshold is the result of the energy cuts applied in the trigger part of the detector. Most of the events are located at low energy in absorbers 1–5 while kaon decay events are expected to be peaked at a measured energy loss 55 MeV (Fig. 2). A simulation shows that most of the background events are compatible with cosmic rays muons going out of the detector via the side. This background is large in absorbers 1–4 because the veto detector is not large enough to reject triggering particles escaping from the sides of these absorbers.

In a second stage, the background cosmic events have been removed taking into account the energy losses of stopping muons in the absorber part of the telescope. A two-dimensional cut, corresponding to the energy losses of the muons deduced from the simulation, was applied to the two last counting scintillators. The range and deposited energy distributions resulting from such a procedure are presented in Fig. 5. These spectra represent the sum of the data obtained for the three targets studied in this experiment. Comparing these results to the simulation of Fig. 2, it is clear that kaon decays have been observed.

The time distribution of the remaining events after the second step of the analysis for the three targets is shown in Fig. 6. The solid line represents the expected slope for kaon decay. The measured time distribution is in agreement with kaon decay only after 18 ns. For $T_0 \leqslant 5$ ns prompt events are still present and a dead time effect due to the high counting rate for prompt events extends up to 18 ns. This dead time effect is reproduced by a simulation also shown in Fig. 6 with a dead time equal to 80% for $T_0 \leqslant 18$ ns. Figure 7 shows the time decay spectra observed with the ^{12}C, ^{nat}Ti, and ^{181}Ta targets for $T_0 > 15$ ns. These spectra seem compatible with kaon time decay spectra represented by solid

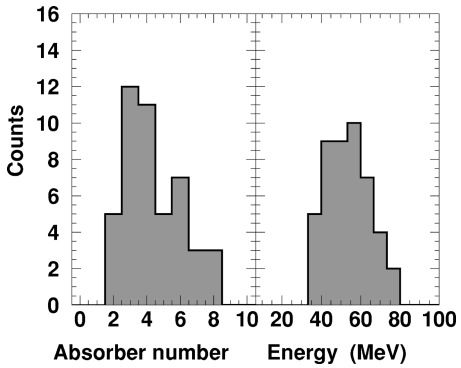

FIG. 5. Observed range and energy deposited in the absorbers for the complete selection. These spectra are a summation of the statistics for the three targets.

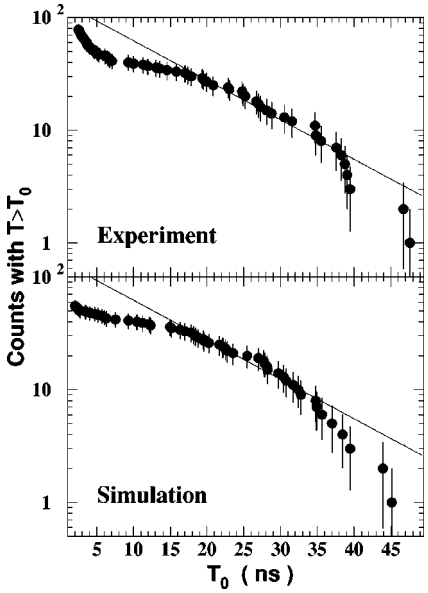

FIG. 6. Time distribution obtained for the complete selection (upper part) and for a simulation (lower part). The solid line corresponds to the time decay of K^+. Prompt events generate a dead time up to 18 ns that is introduced in the simulation.

lines in the figure. This is confirmed by the fits to the decay curve $N_0\exp(-t/\tau)$ performed for the three spectra for $T_0 > 18$ ns which yield $\tau = 18 \pm 12$ ns, 11.5 ± 4.3 ns, and 10.6 ± 2.6 ns for the ^{12}C, ^{nat}Ti, and ^{181}Ta spectra, respectively. Subsequently the mean lifetime of the kaon ($\tau = 12.4$ ns) has been used to derive the number of produced kaons, N_0, from the number of counts observed in the interval 18–50 ns. This gives $N_0 = 23$, 51, and 60 for ^{12}C, ^{nat}Ti, and ^{181}Ta, respectively. The statistical uncertainty in these numbers has been estimated using a simulation. For each target, 10 000 decay time spectra have been generated with an initial number of counts equal to N_0 and a mean lifetime 12.4 ns. Then, a

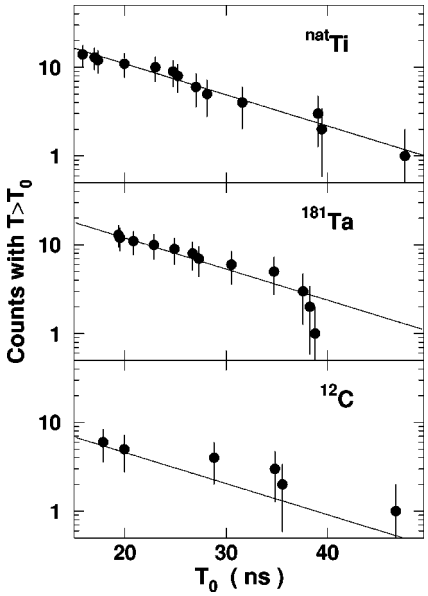

FIG. 7. Time distribution obtained for the three targets for times larger than 15 ns. The solid line corresponds to the decay time of K^+.

TABLE I. Number of kaon production events derived for the three measurements on ^{12}C, ^{nat}Ti, and ^{181}Ta targets.

Target	^{12}C	^{48}Ti	^{181}Ta
N_0	23 (14→37)	51 (37→69)	60 (42→79)

distribution of the estimated initial number of counts N_0^{est} has been obtained from the number of counts in the interval 18–50 ns. To get an approximation of a standard deviation of these discrete N_0^{est} distributions, the next N_0^{est} value corresponding to a value lower than 60% of the maximum of the distribution has been used. The results are reported in Table I.

B. Decorrelated analysis

An analysis based on the total energy spectrum has been performed in order to check the values extracted from the event-by-event analysis. The energy spectrum is composed of good events superimposed on a contamination background which can be estimated using decorrelation techniques. This background arises mostly from high-energy cosmic muons going through the detector. These minimum ionizing particles therefore do not show the correlation of energy losses of stopping muons in the absorbers. The first selection leads to a first sample of about 700 events. Starting from this first sample, eight classes of events are constructed associated with each stopping absorber number (A_1–A_8). For an event of a given class with a decay time $T > T_0$, a decorrelated event is then constructed by a random sampling (excluding the parameters of the physical event) of the energy loss in the detection planes. All the events are treated in the same way, producing a decorrelated energy distribution associated with a decay time $T > T_0$. This distribution is normalized to the lower part of the initial energy distribution (≈ 25 MeV) where the muons of interest are not expected to contribute. The two energy spectra are subtracted, allowing the number of counts with a decay time $T > T_0$ to be evaluated. The time spectrum deduced from this method is presented in Fig. 8. The global features of the time spectrum are similar for both analyses (event by event, Fig. 6, and decorrelated, Fig. 8). Parametrizing the decorrelated time spectrum by $N_0\exp(-t/\tau)$ gives $N_0 = 143 \pm 53$ and $\tau = 14.6 \pm 3.0$. The solid line in Fig. 8 is the result of this exponential fit. The

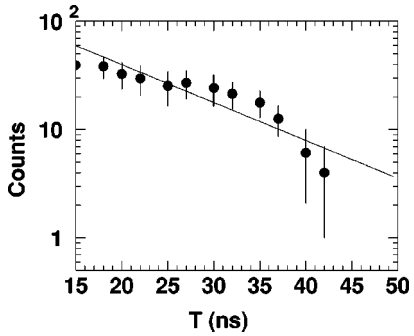

FIG. 8. Time distribution obtained by the decorrelation analysis (see text) based on a global data reduction of the energy spectra.

TABLE II. Cross sections for K^+ production for the ^{12}C, ^{nat}Ti, and ^{181}Ta targets for three assumptions: (1) isotropic emission in the laboratory frame with a kinetic energy $T_K = 35$ MeV, (2) isotropic emission in the laboratory frame with a kinetic energy spectrum given by Ref. [11], and (3) isotropic emission in the fireball frame with a kinetic energy $T_K = 35$ MeV.

Target	$E_{\text{c.m.}}$ (MeV)	$\sigma_{\text{tot}}^{(1)}$ (pb)	$\sigma_{\text{tot}}^{(2)}$ (pb)	$\sigma_{\text{tot}}^{(3)}$ (pb)
^{12}C	820	82	96	107
		(50→131)	(58→154)	(65→172)
^{48}Ti	1870	511	598	571
		(371→691)	(434→808)	(414→722)
^{181}Ta	2744	3093	3616	3358
		(2165→4072)	(2531→4761)	(2351→4421)

event number N_0 is compatible with the number of good events (134) deduced from the previous analysis. From this result one can conclude that there is no loss of events and no background contamination in our data selection. The fitted slope parameter τ is also compatible with the expected slope for K decay of ~ 12.4 ns. The agreement between the two methods give added confidence about the extracted number of events.

IV. RESULTS AND DISCUSSION

A. Derivation of cross sections

In order to extract production cross sections, the K^+ detection efficiencies have been calculated from GEANT simulations including a geometrical description of the experimental set-up and assuming three different production modes: (1) isotropic emission in the laboratory frame with a kinetic energy $T_K = 35$ MeV, (2) isotropic emission in the laboratory frame with a kinetic energy spectrum as reported elsewhere [11] and (3) isotropic emission in the fireball frame with a kinetic energy $T_K = 35$ MeV.

In the above calculations of the detection efficiencies, corrections for the particle decay are also included. The total cross sections thus obtained are presented in Table II and labeled (1), (2), or (3) according to the three different production modes described above. The values in parentheses are the upper and lower limits of the total cross sections, taking into into account the statistical errors. The total cross sections are very little influenced by the assumed emission patterns and remain inside the limits of experimental errors, independently of the kaon energetic distribution and Jacobian effects. In the following we use the cross sections calculated assuming isotropic emission in the laboratory with a kinetic energy $T_K = 35$ MeV. The target mass dependence of the total cross section has been fitted by a power of A. We obtain $x = 1.34 \pm 0.22$ for the power of A. This result differs from the $A_T^{2/3}$ scaling observed in π production in the same energy range. This could be a consequence of the different absorption of pions and kaons.

B. Participant-spectator model

Experimental data [2,3,15,16] suggest that pions are emitted from a composite system formed by the overlap between the projectile and the target nuclei using the geometrical concepts of the fireball participant-spectator model [17]. The size of the composite system is then a function of the impact parameter. Pion production is possible only if the c.m. energy of the composite system (excitation energy) is such that $E^* \geqslant m_\pi$. This sets an upper limit for the impact parameter (b_{eff}) which is determined by energetic considerations.

The mean number of participant nucleons averaged over the impact parameters is, respectively, 10, 20, and 39 for ^{12}C, ^{48}Ti, and ^{181}Ta targets and ^{36}Ar projectile. The mean value of the c.m. energy is, respectively, 215, 435, and 715 MeV. The mean c.m. energy of the participants is given by

$$\langle E_{\text{c.m.}} \rangle = (m^2 \langle N_{pt} \rangle^2 + 2mE_{\text{lab}} \langle N_p \rangle \langle N_t \rangle)^{1/2} - m \langle N_{pt} \rangle,$$

with $\langle N_p \rangle = A_P A_T^{2/3}/(A_P^{1/3} + A_T^{1/3})^2$ and $\langle N_t \rangle = A_T A_P^{2/3}/(A_P^{1/3} + A_T^{1/3})^2$ representing the mean number of participant projectile and target nucleons, respectively ($m = 931.5$ MeV, $\langle N_{pt} \rangle = \langle N_p \rangle + \langle N_t \rangle$, and $E_{\text{lab}} = 92$ MeV/nucleon). The mean c.m. energy of the participants is lower than the kaon production absolute energy threshold (671 MeV), except for the heaviest system, but the c.m. energy of the participants depends on the impact parameter:

$$E_{\text{c.m.}}(b) = [m^2 N_{pt}(b) + 2mE_{\text{lab}} N_p(b) N_t(b)]^{1/2} - mN_{pt}(b),$$

where $N_p(b)$ and $N_t(b)$ are calculated using the geometrical concepts of the fireball participant-spectator model [17]. This dependence is shown in Fig. 9. By requiring that the c.m. energy satisfy $E_{\text{c.m.}}(b) \geqslant 671$ MeV, we obtain upper limits for the impact parameter b of $b_{\text{eff}}/(R_p + R_t) = 0.22$, 0.54, and 0.70 for ^{12}C, ^{48}Ti, and ^{181}Ta targets, respectively. Weighting with $b(b = 0 \rightarrow b_{\text{eff}})$, it is possible to evaluate the mean number of participating projectile and target nucleons in the range $0 \rightarrow b_{\text{eff}}$ which is determined by energetic considerations. In Table III, the calculated results for $\langle E_{\text{c.m.}} \rangle$, $\langle N_{pt} \rangle$, and $\langle \varepsilon^* \rangle = \langle E_{\text{c.m.}}/\text{nucleon}_{pt} \rangle$ are shown for our three systems. In the last column of Table III, the kaon production probabilities defined as $P_{\text{eff}} = \sigma_{\text{exp}}/(\sigma_{\text{eff}} \langle N_{pt} \rangle_{\text{eff}})$ are reported where $\sigma_{\text{eff}} = \pi b_{\text{eff}}^2$.

For the three systems, the mean excitation energies of the composite system are similar. The cross section increases with the size of the intermediate zone, but the probability remains constant in the limit of experimental errors. In view

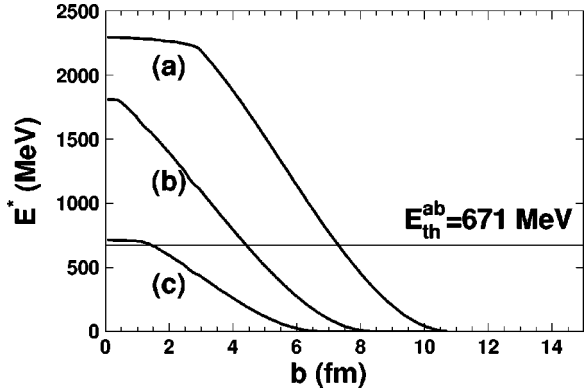

FIG. 9. Excitation energy of the fireball as a function of the impact parameter of the reactions (a) ^{36}Ar+^{181}Ta, (b) ^{36}Ar +^{nat}Ti, and (c) ^{36}Ar+^{12}C at 92 MeV/nucleon. The absolute energy threshold to produce a kaon (671 MeV) is indicated by a solid line.

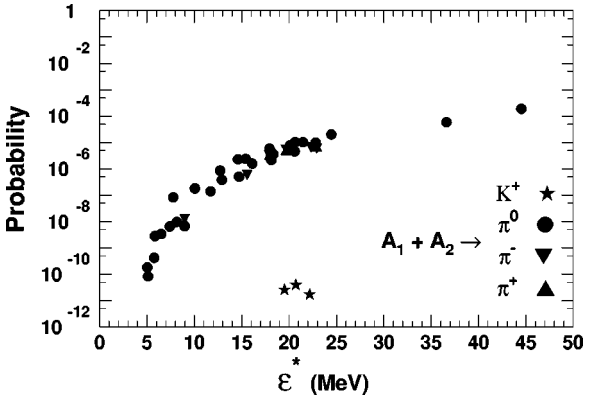

FIG. 10. Meson production probability per participant nucleon as a function of the effective excitation energy ϵ^* defined in the text.

of the uncertainties of fixing b_{eff}, the correlation between excitation energy and production probability gives support to the validity of the geometrical concepts used to define the assumed kaon sources. In spite of the uncertainties in the evaluation of $\langle \varepsilon^* \rangle$, an energy scaling is observed in the pion production probability [18–30] (Fig. 10). This approach leads to a ratio $K/\pi \simeq 10^{-6}$ at $\langle \varepsilon^* \rangle \simeq 20$ MeV which is consistent with a model [11] wherein production cross sections are calculated in the framework of a cooperative mechanism.

C. Comparison with existing data

In meson production analysis, it is usual to present the experimental cross section in terms of the probability per participant nucleon. This probability is given by

$$P_i = \frac{\sigma_{\text{expt}}}{\sigma_g \langle A_p \rangle},$$

with σ_{expt} being the experimental cross section, σ_g the geometrical cross section, and $\langle A_p \rangle_b$ the mean number of participant nucleons. The geometrical cross section is expressed as

$$\sigma_g = \pi r_0^2 (A_P^{1/3} + A_T^{1/3})^2,$$

with A_P and A_T the mass numbers of the projectile and target nuclei, $r_0 = 1.2$ fm and

$$\langle A_p \rangle = \frac{A_P A_T^{2/3} + A_T A_P^{2/3}}{(A_P^{1/3} + A_T^{1/3})^2}.$$

TABLE III. Characteristics of the the reactions of ^{36}Ar ions on targets of ^{12}C, ^{nat}Ti, and ^{181}Ta at 92 MeV/nucleon incident energy.

Target	$\langle N_{pt} \rangle$	$\langle E_{\text{c.m.}} \rangle$ MeV	$\langle \varepsilon^* \rangle$ MeV/nucleon	P_{eff}
^{12}C	33.7	696	20.7	$(3.9 \pm 1.8) \times 10^{-11}$
^{48}Ti	49.3	1090	22.6	$(1.6 \pm 1.1) \times 10^{-11}$
^{181}Ta	73.8	1439	19.5	$(2.4 \pm 0.6) \times 10^{-11}$

Similarities in the subthreshold production of strange and nonstrange mesons can be seen with the universal dependence of the meson production probability per participant nucleon, if this probability is plotted as a function of the Coulomb-corrected bombarding energy per nucleon normalized to the energy threshold in free N-N collisions [10].

The excitation function for π and K^+ production in $A+A$ collisions is presented in Fig. 11. The present data (the lowest-energy data points) follow the trend given by previously measured data (π and K^+) [7,18–30]. In this picture, the probability per participant nucleon to produce either a pion or a kaon is very similar at equivalent relative energy $[(E - V_C)/A]/E_{\text{th}}^{NN}$ whatever the strangeness of the meson. When discussing subthreshold meson production in heavy ion reactions, it should be borne in mind that the definite threshold in a fully coherent production is given by

$$E_{\text{th}}^{\text{def}} = \frac{E_{\text{th}}^2 + 2(A_p + A_t) m E_{\text{th}}}{2 m A_p A_t},$$

where $E_{\text{th}} = 140$ and 671 MeV, respectively, for pion and kaon production. Then we observe that

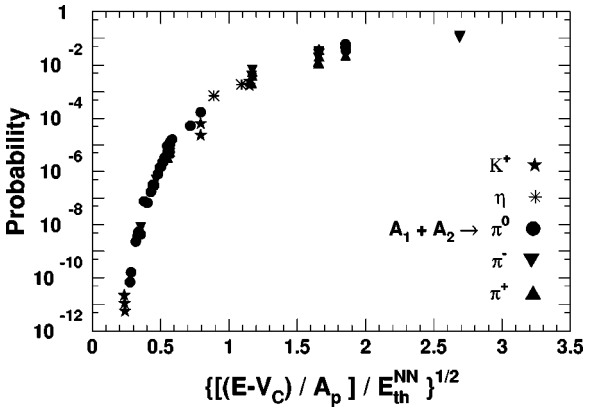

FIG. 11. Meson production probability per participant nucleon as a function of square root of the Coulomb corrected bombarding energy per nucleon normalized to the nucleon-nucleon energy threshold for nucleus-nucleus collisions.

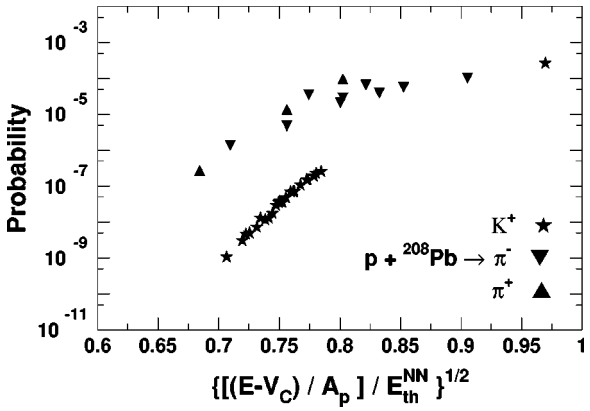

FIG. 12. Pions and kaons production probability as a function of the square root of the Coulomb corrected bombarding energy per nucleon normalized to the nucleon-nucleon energy threshold for the reaction $p+{}^{208}\mathrm{Pb}$.

$$\frac{(E_{\mathrm{th}}^{\mathrm{def}})^{\pi}}{(E_{\mathrm{th}}^{\mathrm{def}})^{K}} \sim \frac{(E_{\mathrm{th}})^{\pi}}{(E_{\mathrm{th}})^{K}} \sim \frac{(E_{\mathrm{th}}^{NN})^{\pi}}{(E_{\mathrm{th}}^{NN})^{K}}.$$

The observed universality is mainly due to the weak variation of the π and K threshold ratio with respect to the energetic conditions of production. Thus the agreement of our data with the universal dependence of meson production [10] does not allow any conclusions about the processes involved in meson production but it is very useful to predict experimental cross sections.

This is confirmed by an analysis of π and K^+ production in p-nucleus reactions near the absolute threshold (140 MeV for π and 671 MeV for K). Using the same approach, we observe (Fig. 12) a large gap between the two excitation functions. The ratio of the production probabilities in $p+\mathrm{Pb}\rightarrow\pi^0$ and $p+\mathrm{Pb}\rightarrow K^+$ is about 10^3 and is comparable to the cross section ratio of the elementary processes $N+N\rightarrow N+N+\pi$ and $N+N\rightarrow N+\Lambda+K$. Thus, the π and K production for p-nucleus collisions near the absolute threshold can be explained as a convolution of the elementary cross section of the p-nucleon system using high-momentum components of the nuclear wave function [1,31–33]. The K^+ production results from a dominant two-step mechanism [31,33] in the collision of secondary pions ($p+N\rightarrow\pi+\cdots$) with the nucleons inside the nucleus ($\pi+N\rightarrow\Lambda+K^+$). From these results, the conclusion is that π and K production in p-nucleus reactions is dominated by the N-N elementary process.

K^+ and π production at bombarding energies of 92 MeV/nucleon and 20 MeV/nucleon, respectively, would be comparable, considering just the ratios between the incident energy per nucleon and the N-N production energy threshold. But in a 20 MeV/nucleon collision, the available energy in the N-N system is about 140 MeV when taking into account an internal momentum of 350 MeV/c (Fig. 13). Then subthreshold pion production is energetically possible. However, in a 92 MeV/nucleon collision, with the same internal momenta, the available energy is about 210 MeV, far from the kaon center-of-mass threshold energy (671 MeV). This value is reached only by taking into account an internal momentum of 800 MeV/c in both partner nuclei (Fig. 13).

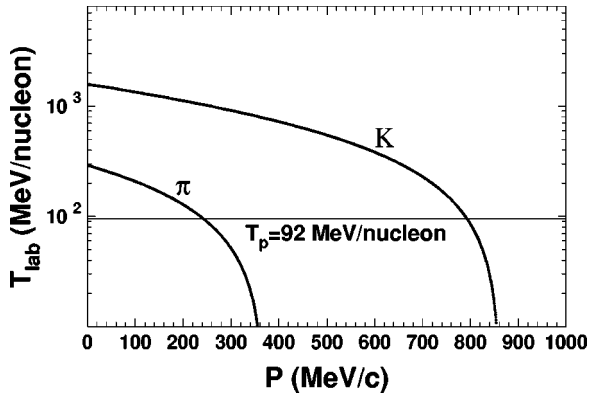

FIG. 13. Correlation of the incident beam energy and of the internal momentum of nucleons necessary in both nuclei to produce a pion or a kaon.

These estimates have been made in the most favorable kinematical configuration: a collision between a projectile nucleon with an internal velocity vector (beam+Fermi) aligned with the relative velocity and a target nucleon with a Fermi velocity in the opposite direction. The distribution of the internal momentum of nucleons in a nucleus deduced from experimental distributions [34] fall down about three orders of magnitude from $P_f=350$ MeV/c to $P_f=800$ MeV/c. In the case under consideration the probabilities to produce K^+ and π cannot be of the same order of magnitude. At an energy as low as 25 MeV/nucleon, the simple Fermi motion cannot explain the measured pion cross section [35]. There is a need to call for cooperative modes of several participant nucleons to satisfy energy conservation [36,37]. Similar conclusions can be deduced from K^+ production at 92 MeV/nucleons.

V. CONCLUSIONS

Kaon decays have been observed in the collisions of 92 MeV/nucleon ^{36}Ar with ^{12}C, $^{\mathrm{nat}}$Ti, and ^{181}Ta, and values of the total kaon production cross section have been derived using an event-by-event analysis and assuming isotropic emission. A statistical analysis applying correlation techniques to the various energy loss measurements shows that no significant loss of events occurred and that background contamination can be excluded. The variation of the K^+ production cross section with target mass number follows a $A_{\mathrm{T}}^{1.33}$ scaling law, larger than the $A_{\mathrm{T}}^{2/3}$ one observed for the pion production. The target dependence of two calculations [11,12], reproducing the order of magnitude of the cross section for the titanium target, remains to be investigated.

The present results follow the general trend given by the universal dependence of meson production [10]. This agreement does not allow final conclusions regarding the precise processes leading to meson production. Taking into account a reasonable Fermi momentum, pion and kaon production in nucleon-nucleus collisions are compatible with anucleon-nucleon initiated production. Similar considerations in nucleus-nucleus production rule out a common nucleon-nucleon production mechanism. However, the K production can be consistently described in the framework of a participant-spectator model. In that case, close to the absolute threshold, a cooperative mechanism is required and energetic conditions apply to the effective number of nucleons

involved in the production. If the production probability is restricted to this effective number of nucleons involved in the process, the kaon production probability is lower than the pion production probability as in nucleon-nucleus reactions.

In this experiment, we have demonstrated that kaon production is measurable at incident energies below 100 MeV/nucleon. At such a low energy, geometrical and kinematical constraints play a major role in the kaon production.

[1] W. Cassing, V. Metag, U. Mosel, and K. Nita, Phys. Rep. **188**, 363 (1990).
[2] D. Lebrun *et al.*, Phys. Lett. B **223**, 139 (1989).
[3] J. L. Laville, A. Badala, R. Barbera, G. Bizard, R. Bougault, D. Durand, A. Palmeri, G. S. Pappalardo, and F. Riggi, Nucl. Phys. **A564**, 564 (1993).
[4] J. Ellis and M. Karliner, Phys. Lett. B **341**, 397 (1995).
[5] K. Abe *et al.*, Phys. Rev. Lett. **74**, 346 (1995).
[6] D. Adams *et al.*, Phys. Lett. B **329**, 399 (1994).
[7] S. Schnetzer, M. C. Lemaire, R. Lombard, E. Moeller, S. Nagamiya, G. Shapiro, H. Steiner, and I. Tanihata, Phys. Rev. Lett. **49**, 989 (1982).
[8] D. Miskoviec *et al.*, Phys. Rev. Lett. **72**, 3650 (1994).
[9] J. Julien, D. Lebrun, A. Mougeot, P. de Saintignon, N. Alamanos, Y. Cassagnou, C. Le Brun, J. F. Lecolley, R. Legrain, and G. Perrin, Phys. Lett. B **264**, 269 (1991).
[10] V. Metag, Prog. Part. Nucl. Phys. **30**, 75 (1993).
[11] S. Gosh, Phys. Rev. C **45**, R518 (1992).
[12] M. Belkacem, E. Suraud, and S. Ayik, Phys. Rev. C **47**, R16 (1993).
[13] V. P. Koptev *et al.*, Sov. Phys. JETP **67**, 2177 (1988).
[14] R. Brun *et al.*, CERN Report No. DD/EE/84-1 (unpublished).
[15] B. Erazmus *et al.*, Nucl. Phys. **A481**, 821 (1988).
[16] D. Lebrun, J. Chauvin, J. Julien, C. Le Brun, J. F. Lecolley, G. Perrin, D. Rebreyend, and P. de Saintignon, Z. Phys. A **335**, 73 (1990).
[17] J Gosset, H. H. Gutbrod, W. G. Meyer, A. M. Poskanzer, A. Sandoval, R. Stock, and G. D. Westfall, Phys. Rev. C **16**, 629 (1977).
[18] E. Grosse, Prog. Part. Nucl. Phys. **30**, 89 (1993).
[19] M. Prakash, P. Braun-Munzinger, and J. Stachel, Phys. Rev. C **33**, 937 (1986), and references therein.
[20] G. Sanouillet *et al.*, Nuovo Cimento A **99**, 875 (1988).
[21] S. Y. Fung, W. Gorn, G. P. Kiernan, F. F. Liu, J. J. Lu, Y. T. Oh, J. Ozawa, R. T. Poe, L. Schroeder, and H. Steiner, Phys. Rev. Lett. **40**, 292 (1978).
[22] A. Sandoval, R. Stock, H. E. Stelzer, R. E. Renfordt, J. W. Harris, J. P. Brannigan, J. V. Geaga, L. J. Rosenberg, L. S. Schroeder, and K. L. Wolf, Phys. Rev. Lett. **45**, 874 (1980).
[23] K. A. Frankel *et al.*, Phys. Rev. C **32**, 975 (1985).
[24] E. Chiassa *et al.*, Nucl. Phys. **A422**, 621 (1984).
[25] V. Bernard *et al.*, Nucl. Phys. **A423**, 511 (1984).
[26] S. Nagamiya, M.-C. Lemaire, E. Moeller, S. Schnetzer, G. Shapiro, H. Steiner, and I. Tanihata, Phys. Rev. C **24**, 971 (1981).
[27] G. R. Young, F. E. Obenshain, F. Plasil, P. Braun-Munzinger, R. Freifelder, P. Paul, and J. Stachel, Phys. Rev. C **33**, 742 (1986).
[28] P. Braun-Munzinger, P. Paul, L. Ricken, J. Stachel, P. H. Zhang, G. R. Young, F. E. Obenshain, and E. Grosse, Phys. Rev. Lett. **52**, 255 (1984).
[29] H. Heckwolf *et al.*, Z. Phys. A **315**, 243 (1984).
[30] H. Noll *et al.*, Phys. Rev. Lett. **52**, 1284 (1984).
[31] A. A. Sibitsev and M. Büsher, Z. Phys. A **347**, 191 (1994).
[32] W. Cassing *et al.*, in Proceedings of the 7th International Conference on Nuclear Reaction Mechanisms, Varenna, 1994, p. 544.
[33] M. Debowski *et al.*, Z. Phys. A **356**, 313 (1996).
[34] J. V. Geaga, S. A. Chessin, J. Y. Grossiord, J. W. Harris, D. L. Hendrie, L. S. Schroeder, R. N. Treuhaft, and K. Van Bibber, Phys. Rev. Lett. **45**, 1993 (1980).
[35] J. Stachel *et al.*, Phys. Rev. C **33**, 1420 (1986).
[36] R. Shyam and L. Knoll, Nucl. Phys. **A426**, 606 (1984).
[37] C. Guet and M. Prakash, Nucl. Phys. **A428**, 1196 (1984).